Efficient Hybrid Solar Cells Based on Solution Processed Mesoporous TiO_2 / Tin (II) Sulfide Heterojunctions

*Dong Ding[1], Thomas Rath[1,2], Luis Lanzetta[1], Jose Manuel Marin-Beloqui[1], Saif A. Haque[1]**

[1] Department of Chemistry and Centre for Plastic Electronics, Imperial College London, Imperial College Road, London, SW7 2AZ, UK

[2] Institute for Chemistry and Technology of Materials, NAWI Graz, Graz University of Technology, Stremayrgasse 9, 8010 Graz, Austria

Corresponding Author

*E-mail: s.a.haque@imperial.ac.uk

ABSTRACT. Tin monosulfide (SnS) is emerging as a promising absorber material for the development of low cost, solution-processable solar cells. Herein, we present a straight-forward, solution-based route for the preparation of tin monosulfide (SnS) films employing a green solvent, namely tetrahydrofuran (THF). We show that the surface coverage and the morphology of the SnS films can be tuned by modification of the precursor solution composition and film deposition conditions. Furthermore, we explore the effect of a PEDOT:PSS interlayer and fabricate solar cells based on the following architecture: FTO/planar-TiO_2/mesoporous-TiO_2/SnS/P3HT/PEDOT:PSS/Ag. Devices based on this architecture are shown to exhibit power conversion efficiencies (PCEs) of 3.0%, thus demonstrating the potential of our method for the development of low-cost and environmentally friendly solar cells.

KEYWORDS. (tin monosulfide (SnS), thin film solar cells, hybrid solar cells, solution processed deposition, morphology, mesoporous TiO_2)

In the past few decades, thin film solar cells based on metal chalcogenides have gained growing interest in the research field as alternatives to conventional crystalline silicon solar cells. The most prominent examples of thin film technologies are CdTe and copper indium gallium selenide (CIGS), which exhibit competitive power conversion efficiencies with silicon solar cells.[1] However, the fabrication of efficient CIGS or CdTe solar cells requires the use of vacuum or high temperature and these materials contain elements in limited supply, leading to high production costs. As such, there is a need to develop new thin film materials that can be used in solar energy conversion devices.

Tin sulfide (SnS) has emerged as a promising solar cell material, as a replacement candidate for more conventional thin film absorbers such as CdTe and CIGS.[2–5] In particular, SnS has attracted increasing attention due to its potential for cost-competitive, large-scale and environmentally friendly photovoltaic applications. As a solar cell absorber, SnS has a high optical absorption coefficient ($>10^4$ cm^{-1}) and an ideal band gap of 1.3 eV.[6–7] In addition, SnS is known to be stable under ambient conditions and also exists in nature as a mineral, Herzenbergite; therefore, SnS has better prospects in terms of stability compared to other technologies such as hybrid lead halide perovskite and organic solar cells. For example, in a recent study, it was found that the PCE of a SnS-based solar cell kept almost constant during storage in air for six months without encapsulation.[8] Furthermore, SnS solar

cells are less toxic as compared to thin film solar cells that comprise toxic elements such as cadmium or lead.

A variety of deposition methods have been developed and utilized for the preparation of SnS thin films, including chemical vapor deposition (CVD), thermal evaporation, chemical sputtering, vapor-transport deposition (VTD), spray deposition, successive ionic layer adsorption reaction (SILAR), chemical bath deposition (CBD), and atomic layer deposition (ALD).[2,8–12] To date, the most efficient SnS solar cells reveal PCEs of 2.9% to 4.4% and have SnS absorber layers prepared via VTD,[8] ALD,[13] thermal evaporation,[14] or CVD.[15] However, these deposition methods require vacuum, high temperature or slow deposition rates; thus, they are not ideal for large-scale production. Motivated by this, in our previous work we reported a solution-processed fabrication technique for SnS thin film solar cells.[16] Specifically, SnS films were fabricated from a pyridine solution containing $SnCl_2$ and thioacetamide. Planar heterojunction solar cells based on such SnS layers were shown to exhibit a short circuit current (J_{sc}) of 11.6 $mAcm^{-2}$, open-circuit voltage (V_{oc}) of 0.276 V and fill factor of 0.38, leading to a PCE of 1.2%. However, the performance of these solar cells is most likely limited by poor surface coverage / morphology of the SnS absorber on TiO_2. For example, a poor coverage would be expected to limit the light harvesting efficiency as well as lead to pin holes / shorting pathways that may serve to reduce the photovoltage and fill factor of the solar cell. As such, it is

reasonable to suppose that improvements in device performance can be realized by optimization of the surface coverage and morphology of the SnS absorber layer.

In this paper, we build on our previous work and report an alternative fabrication route to tin (II) sulfide (SnS) films that enables better control of film coverage and morphology. Moreover, we extend this approach to the fabrication of SnS layers on high surface area, mesoporous TiO_2 electrodes. Transient absorption spectroscopy is used to study charge separation and recombination at mesoporous-TiO_2/SnS/P3HT heterojunctions. Furthermore, we fabricate solar cells with such heterojunctions and show that the integration of a PEDOT:PSS interlayer between P3HT and the hole collecting metal electrode leads to devices that exhibit power conversion efficiencies of 3% under simulated AM 1.5G solar illumination.

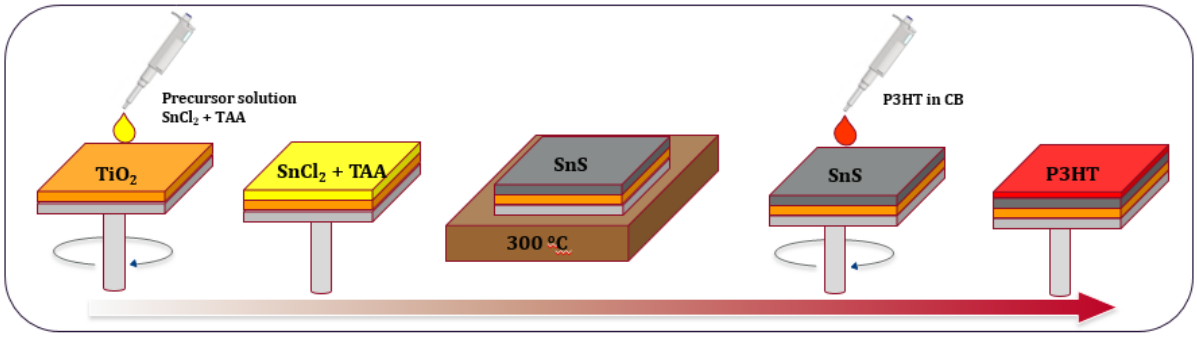

Figure 1. Schematic illustration of the spin coating and heating steps for the preparation of the TiO_2/SnS/P3HT layers.

We first consider the fabrication of SnS thin films. The spin coating procedure employed herein to fabricate the films is schematically described in **Figure 1**. A stable precursor solution was formed by dissolving two starting materials, $SnCl_2$ and thioacetamide in tetrahydrofuran (THF). The resulting precursor solution lasted for more than seven days without any degradation. The precursor solution was spin coated on mp-TiO_2 films to afford a precursor layer, which was then converted to a SnS layer via thermal annealing at 300 ^oC under N_2 atmosphere. During the annealing process, thioacetamide decomposes to release H_2S gas which serves as the sulfur source and reacts with the Sn^{2+} ions in the precursor layer to form a grey-coloured SnS film. We note that the other by-products are volatile and leave the film during annealing.

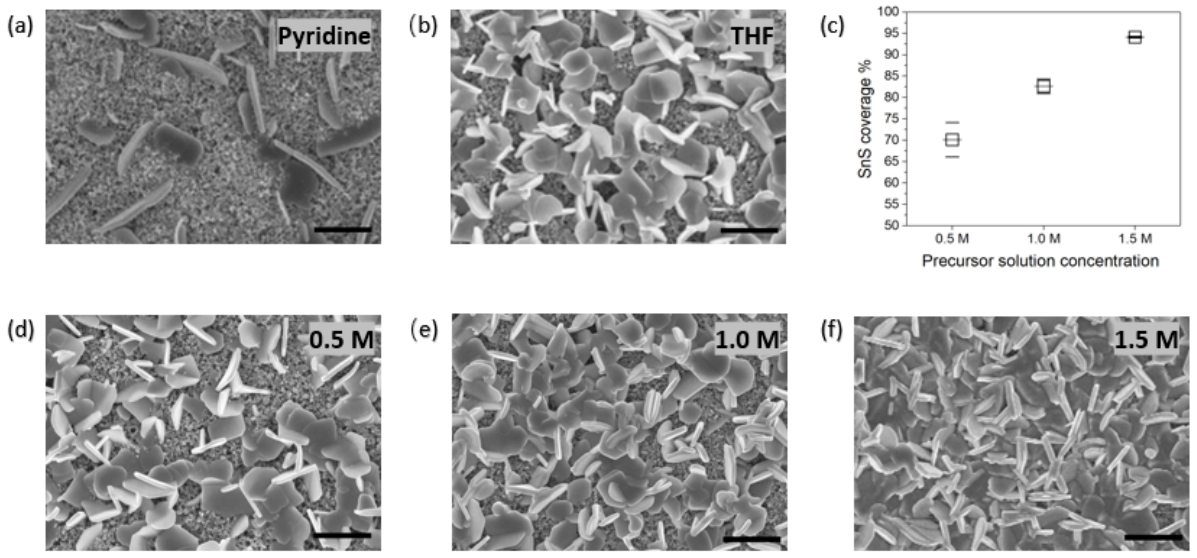

Figure 2. Top-view SEM images of SnS films prepared from solvent (a) pyridine and (b) THF. (c) SnS surface coverage extracted from the SEM images plotted against the concentration of precursor

solution of SnS. SEM images of the SnS films prepared with varying precursor solution concentrations: (d) 0.5 M, (e) 1.0 M, and (f) 1.5 M. The scale bars denote 1 μm.

Figure 2a and 2b show top-view scanning electron microscope (SEM) images of SnS layers deposited on mesoporous TiO_2 films from two different solvent systems, namely pyridine and THF. As can be seen in Figure 2a, the SnS film prepared from pyridine, exhibits large voids between the nanoplates, indicating incomplete coverage of the mesoporous-TiO_2 layer with SnS; this being in agreement with previous work.[16] A SEM image of SnS films processed from THF is presented in Figure 2b. The films prepared from THF comprise SnS nanoplates with an average size of 800 nm. Importantly, the SnS films processed from THF show a significantly better coverage relative to the films processed from pyridine. It is also noted that the SnS layer contains a porous network of nanoplates which take random orientations. Figure S1 shows a cross-sectional SEM image of SnS layer. This porous structure provides a high surface area and enables the organic hole transporting material to infiltrate inside the pores to form organic – inorganic semiconductor heterojunction *vide infra*.

Further optimization of the surface coverage and morphology was achieved by varying the concentration of the precursor solution and therefore the thickness of the absorber layer. The relationship between surface coverage and precursor concentration is presented in Figure 2c, these

data suggest increasing the precursor concentration from 0.5 M to 1.5 M leads to an improvement in the surface coverage from 70% to 94%. Figures 2d-f show SEM images of SnS prepared from different precursor solution concentrations deposited on mesoporous-TiO_2. The data indicates that increasing the precursor solution concentration leads to fewer pinholes and an increased surface coverage of SnS nanoplates on top of TiO_2. The SEM image of a SnS film made from a 2.0 M precursor solution is shown in Figure S2a and reveals that despite the good solubility of the starting materials in THF, the coverage of synthesized SnS film is not further improved when increasing the concentration of the precursor solution beyond 1.5M.

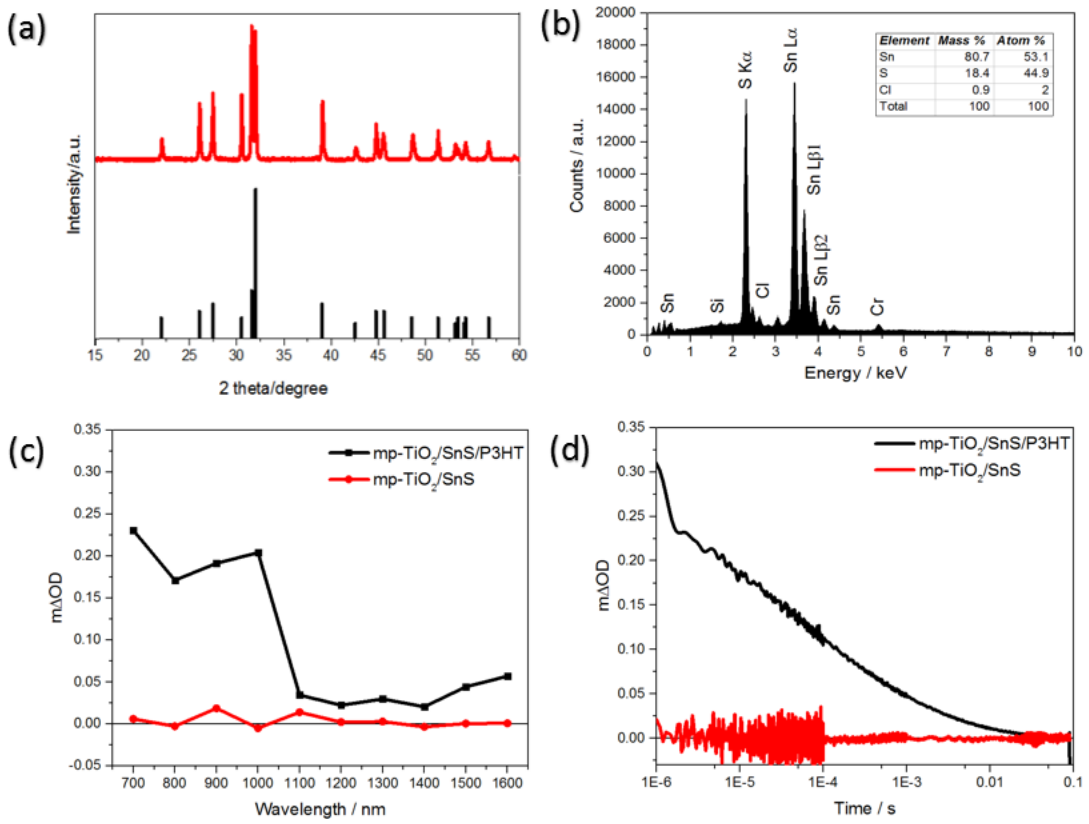

Figure 3. (a) X-ray diffraction patterns: red trace is the measured sample and black trace is the reference pattern (PDF 14-0620). (b) SEM-EDX spectrum of a SnS film prepared from THF. (c) Transient absorption spectra of a SnS and a SnS/P3HT film on mp-TiO_2 measured 10 μs after excitation. (d) Transient absorption kinetics of the same samples recorded at 1000 nm with excitation at 510 nm.

To confirm that our fabrication method leads to the formation of tin (II) sulfide, we resorted to X-ray diffraction (XRD) measurements. As shown in **Figure 3a**, the peaks are sharp and narrow indicating the material synthesized is highly crystalline. More importantly, all peaks match the orthorhombic SnS characteristics (Herzenbergite) without the presence of additional peaks (corresponding to SnS_2 and Sn_2S_3) which have been observed previously when pyridine was used as the precursor solvent.[16]

SEM-EDX measurements were used to study the chemical composition of the prepared SnS films. The data presented in Figure 3b, reveals an atomic ratio for Sn:S of 1.16:1 indicating that the synthesized SnS films are sulfur-deficient. Due to the high volatility of sulfur, sulfur-deficiency is commonly observed in SnS films, especially when annealing is required.[17] The presence of 2% Cl in the sample is caused by the unreacted starting material $SnCl_2$. We note that peaks corresponding to Si

and Cr in the spectrum come from the glass substrate and the Cr coating layer, which was used to prevent charging from the sample by the electron beam during measurement.

Next, the kinetics and yields of photoinduced charge transfer processes in SnS based photoactive layers were interrogated using microsecond transient absorption spectroscopy (μs-TAS). Figure 3c shows transient absorption spectra (mΔO.D. versus wavelength profiles) for mp-TiO_2/SnS/P3HT and mp-TiO_2/SnS samples measured at 10 μs following pulsed laser excitation at 510 nm. In the mp-TiO_2/SnS/P3HT sample (black curve), we attribute the broad transient absorption band between ~ 750 nm – 1050 nm to hole polarons in P3HT; this being in agreement with previous research.[18] In contrast, no transient absorption features are observed in the mp-TiO_2/SnS sample. This could be due to either (i) poor charge separation at mp-TiO_2/SnS heterojunctions or (ii) fast electron – hole recombination in mp-TiO_2/SnS film occurring on timescales faster than the instrument response of the spectrometer. The kinetics of electron – hole recombination in SnS based heterojunctions reported herein were studied by monitoring the decay of the P3HT polaron band at 1000 nm. Figure 3d shows the recombination kinetics for two systems: mp-TiO_2/SnS/P3HT (black curve) and the control sample, namely mp-TiO_2/SnS (red curve). The recombination lifetime, $\tau_{50\%}$ (which we define as time taken for half the polarons to decay back to the ground state) in the mp-TiO_2/SnS/P3HT system was found to be ~150 μs; this being constant with previous work.[16] It is pertinent to note that the change in optical

density (mΔO.D.) plotted on the y-axis in Figure 3d is directly related to the concentration of photogenerated species and is therefore a measure of the yield of charge separation. It is clear from the data presented in Fig 3c and 3d, that the mp-TiO_2/SnS/P3HT films exhibit a higher yield of charge separation relative to mp-TiO_2/SnS films. Moreover, Figure S3a (green curve) presents the transient absorption kinetics obtained in Al_2O_3/SnS/P3HT films. In this sample, the high conduction band edge of Al_2O_3 (as compared to TiO_2) precludes electron injection from SnS to the metal oxide. Therefore, the transient signal observed in Al_2O_3/SnS/P3HT is most likely due to hole transfer from SnS to P3HT. Taken together, the data presented in Figure 3c and S3a suggests that, in part, photoinduced charge separation in our mp-TiO_2/SnS/P3HT films is initiated by hole transfer from SnS to P3HT. We note that similar behaviour has been reported in other metal sulfide / polymer assemblies such as Sb_2S_3/P3HT films and CdS QD / polymer blends.[19-23] We note that it is possible that photoinduced charge separation via electron trasnfer form the excited state of P3HT to SnS and/or TiO_2 may also contribute to the $P3HT^+$ TAS signal presented in Figure 3d However, we believe that the signal observed herein is mainly due to hole transfer from SnS to P3HT. This is supported by the solar cell performance data reported herein as discussed later.Furthermore, it is pertinent to note that the size of the TAS signal in the mesoporous sample in Figure 3d is three-fold greater in magnitude relative to

that previously observed in the planar sample.[16] This is most likely due to an improved interface and the mesoporous nature of the film providing a high surface area of charge separation to take place.

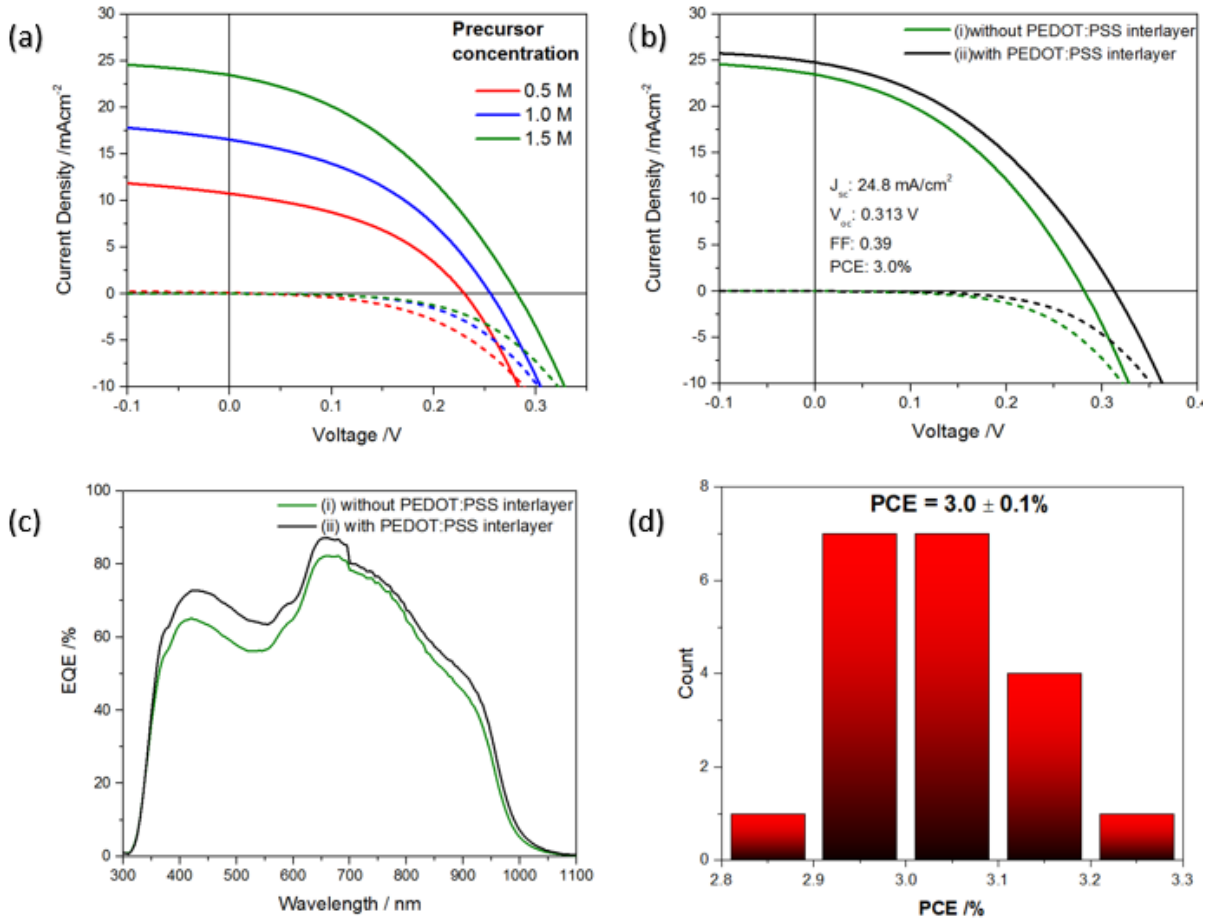

Figure 4. (a) Characteristic J-V curves of the solar cells made from different precursor concentrations and measured in dark (dashed lines) and at a standard AM 1.5G solar illumination, 100 $mWcm^{-2}$ (solid lines). (b) J-V characteristics measured in dark conditions (dashed lines) and under AM 1.5G illumination (solid lines). (c) External quantum efficiency spectra for devices i) without and ii) with a PEDOT:PSS interlayer. (d) Histogram of PCE of 20 solar cells with the structure: mp-TiO_2/SnS/P3HT/PEDOT:PSS/Ag.

We now turn our attention to the photovoltaic performance of devices based on the SnS layers reported herein. Solar cells with the following architecture: glass/FTO/planar-TiO_2/mp-TiO_2/SnS/P3HT/Ag were fabricated and their optoelectronic properties were studied. **Figure 4a** shows current-voltage (J-V) characteristics measured in the dark and under 100 $mWcm^{-2}$ AM 1.5G simulated solar illumination of the solar cells made with different SnS layer thicknesses. The corresponding photovoltaic parameters are presented in **Table 1**. It is apparent from the data presented in Figure 4a and Table 1 that we could obtain thicker SnS absorber layers by increasing the concentration of the precursor solution; and increasing the SnS film thickness and thus coverage leads to an improvement in device PCE. In particular, the best-performing device is based on a 525 nm SnS layer which was prepared from the precursor solution (1.5 M) and it gave a PCE of 2.6%. Devices with higher concentration (2.0 M) were also made, but there was no significant improvement in neither coverage nor device efficiency (see Figure S2b). We note, that the use of a mesoporous TiO_2 electron accepting electrode as compared to a planar TiO_2 electrode which was previously studied,[16] leads to an increase in the short circuit current (J_{sc}) from 11.6 $mAcm^{-2}$ to 23.5 $mAcm^{-2}$ and in efficiency from 1.2% to 2.6%. The high short circuit current is commonly observed in SnS-based solar cells, which in turn is attributed to its broad absorption over the solar spectrum and near ideal band gap. To the best of our knowledge the photocurrent of the SnS solar cells reported

herein is the highest reported so far for SnS-based inorganic-organic hybrid solar cells. On the other hand, the relatively modest open circuit voltage (V_{oc}) and fill factor, presents a challenge to the optimization of SnS based devices.

Table 1. Performance characteristics of the devices prepared with different precursor solution concentrations. The average parameters are values of 20 devices. The device area is 0.10 cm^2.

Precursor concentration	**SnS layer thickness [nm]**		**J_{sc} [$mAcm^{-2}$]**	**V_{oc} [V]**	**FF**	**Efficiency [%]**
0.5 M	170	Avg.	10.8 ± 1.3	0.213 ± 0.03	0.36 ± 0.03	0.9 ± 0.1
		Best	10.7	0.230	0.41	1.0
1.0 M	350	Avg.	16.8 ± 1.8	0.261 ± 0.01	0.38 ± 0.02	1.6 ± 0.1
		Best	16.5	0.256	0.41	1.7
1.5 M	525	Avg.	23.5 ± 0.9	0.285 ± 0.01	0.38 ± 0.01	2.55±0.1
		Best	23.5	0.282	0.39	2.6

In order to improve the open circuit voltage in our devices, we explored the effect of a PEDOT:PSS interlayer. To this end, we fabricated devices with the following architecture: glass/FTO/planar-TiO_2/mp-TiO_2/SnS/P3HT/PEDOT:PSS/Ag. As can be seen in Figure 4b, inserting a thin layer of PEDOT:PSS between P3HT and the Ag electrode increases the short circuit current from 23.5 to 24.8 mA/cm^2 as well as the open circuit voltage from 282 mV to 313 mV, leading to an

increase in PCE from 2.6% to 3.0%. Figure 4c shows the external quantum efficiency (EQE) spectra of the devices made without and with the interlayer of PEDOT:PSS. The peak of the EQE is over 85% and the spectrum still shows significant photocurrent generation at wavelength between 700 and 1000 nm where SnS is the only absorbing material. The band gap of SnS was calculated to be 1.34 eV from the EQE. It is also apparent that the use of a PEDOT:PSS interlayer, leads to an improvement in EQE across the entire energy range as well as an overall increase in the PCE of the device. Histogram of the device efficiencies of 20 solar cells prepared with PEDOT:PSS interlayer is shown in the Figure 4d, and histograms of other device parameters are shown in Figure S4. The devices exhibit an average PCE of 3.0% (max. 3.2%) with small standard deviations in all characteristic parameters, suggesting that our approach gives highly reproducible solar cells. It should be also noted that these devices exhibit the highest reported PCEs for solution-processed SnS-based solar cells. At present, we can only speculate on the origin of these findings. However, three possible mechanisms could explain why a thin interlayer of PEDOT:PSS between P3HT and Ag can improve the performance of the SnS based solar cells. The first mechanism involves PEDOT:PSS acting as a hole extraction layer. To this end, PEDOT:PSS exhibits a work function of 5.0 eV so it can help with energy level matching between P3HT and silver metal contact which has a work function of 4.5 to 4.7 eV respectively. The second possible reason is that the surface of the SnS layer is relatively rough due to the large size of the

nanoplates, and an interlayer of PEDOT:PSS could further smooth the porous SnS-P3HT surface, leading to improved V_{oc} and fill factor. The reason could be that PEDOT:PSS acts as a protection layer for P3HT during silver evaporation process.

In summary, we have fabricated SnS thin film solar cells based on mesoporous TiO_2/SnS/P3HT heterojunctions with PCEs of up to 3.0%. The SnS layers are fabricated using a solution based processing method that enables the film morphology and coverage to be tuned. The synthesis of pure SnS without any secondary phases was confirmed using XRD and SEM-EDX. The charge generation properties at the TiO_2/SnS/P3HT heterojunction were studied using TAS. The performance of the device performance was found to be improved by inserting a PEDOT:PSS interlayer, which allows efficient hole extraction and protects the organic material during metal contact evaporation. Further investigation in the role of the interlayer is still ongoing in our laboratory in order to overcome the limited photovoltage. Finally, we note that preliminary stability studies on pristine SnS films indicate that such layers are stable when exposed to light under ambient environmental conditions (Figure S5). Therefore, we believe that further optimization of the SnS film morphology as well as the supporting device architecture should lead to the realization of a highly efficient and stable photovoltaic device technology.

ASSOCIATED CONTENT

Supporting Information

The Supporting Information is available free of charge on the ACS Publications website.

Materials and methods, SEM image of SnS film prepared from a precursor solution with concentration of 2.0 M, J-V curves of the solar cells made from precursor concentrations of 1.5 M and 2.0 M, TAS kinetics and absorption spectrum of the sample SnS/P3HT film on mp-TiO_2 and mp-Al_2O_3, histograms of device parameters of 20 solar cells.

AUTHOR INFORMATION

Corresponding Author

*E-mail: s.a.haque@imperial.ac.uk

Notes

The authors declare no competing financial interest.

ACKNOWLEDGMENT

S. A. H. acknowledges financial support from the EPRSC via EP/ M023532/1, EP/K010298/1 and EP/K030671/1 grants. Financial support from the Austrian Science Fund (FWF) is acknowledged by TR (grant number: J3515-N20).

REFERENCES

(1) Green, M. A.; Hishikawa, Y.; Warta, W.; Dunlop, E. D.; Levi, D. H.; Hohl-Ebinger, J.; Ho-Baillie, A. W. H. Solar Cell Efficiency Tables (Version 50). *Prog. Photovoltaics Res. Appl.* **2017**, *25* (7), 668–676.

(2) Andrade-Arvizu, J. A.; Courel-Piedrahita, M.; Vigil-Galán, O. SnS-Based Thin Film Solar Cells: Perspectives over the Last 25 Years. *J. Mater. Sci. Mater. Electron.* **2015**, *26* (7), 4541–4556.

(3) Zakutayev, A. Brief Review of Emerging Photovoltaic Absorbers. *Curr. Opin. Green Sustain. Chem.* **2017**, *4*, 8–15.

(4) Guchhait, A.; Dewi, H. A.; Leow, S. W.; Wang, H.; Han, G.; Suhaimi, F. Bin; Mhaisalkar, S.; Wong, L. H.; Mathews, N. Over 20% Efficient CIGS–Perovskite Tandem Solar Cells. *ACS Energy Lett.* **2017**, *2* (4), 807–812.

(5) Kurley, J. M.; Panthani, M. G.; Crisp, R. W.; Nanayakkara, S. U.; Pach, G. F.; Reese, M. O.; Hudson, M. H.; Dolzhnikov, D. S.; Tanygin, V.; Luther, J. M.; Talapin, D.V. Transparent Ohmic Contacts for Solution-Processed, Ultrathin CdTe Solar Cells. *ACS Energy Lett.* **2017**, *2* (1), 270–278.

(6) Ramakrishna Reddy, K. T.; Koteswara Reddy, N.; Miles, R. W. Photovoltaic Properties of SnS Based Solar Cells. *Sol. Energy Mater. Sol. Cells* **2006**, *90* (18–19), 3041–3046.

(7) Schneikart, A.; Schimper, H.-J.; Klein, A.; Jaegermann, W. Efficiency Limitations of Thermally Evaporated Thin-Film SnS Solar Cells. *J. Phys. D. Appl. Phys.* **2013**, *46* (30), 305109.

(8) Lim, D.; Suh, H.; Suryawanshi, M.; Song, G. Y.; Cho, J. Y.; Kim, J. H.; Jang, J. H.; Jeon, C.-W.; Cho, A.; Ahn, S.; Heo, J. Kinetically Controlled Growth of Phase-Pure SnS Absorbers for Thin Film Solar Cells: Achieving Efficiency Near 3% with Long-Term Stability Using an SnS/CdS Heterojunction. *Adv. Energy Mater.* **2018**, 1702605.

(9) Patel, M.; Ray, A. Evaluation of Back Contact in Spray Deposited SnS Thin Film Solar Cells by Impedance Analysis. *ACS Appl. Mater. Interfaces* **2014**, *6* (13), 10099–10106.

(10) Banai, R. E.; Horn, M. W.; Brownson, J. R. S. A Review of Tin (II) Monosulfide and Its Potential as a Photovoltaic Absorber. *Sol. Energy Mater. Sol. Cells* **2016**, *150*, 112–129.

(11) Lewis, D. J.; Kevin, P.; Bakr, O.; Muryn, C. A.; Malik, M. A.; O'Brien, P. Routes to Tin Chalcogenide Materials as Thin Films or Nanoparticles: A Potentially Important Class of Semiconductor for Sustainable Solar Energy Conversion. *Inorg. Chem. Front.* **2014**, *1* (8), 577–598.

(12) Koteeswara Reddy, N.; Devika, M.; Gopal, E. S. R. Review on Tin (II) Sulfide (SnS) Material: Synthesis, Properties, and Applications. *Crit. Rev. Solid State Mater. Sci.* **2015**, *40* (6), 359–398.

(13) Sinsermsuksakul, P.; Sun, L.; Lee, S. W.; Park, H. H.; Kim, S. B.; Yang, C.; Gordon, R. G. Overcoming Efficiency Limitations of SnS-Based Solar Cells. *Adv. Energy Mater.* **2014**, *4* (15), 1–7.

(14) Steinmann, V.; Jaramillo, R.; Hartman, K.; Chakraborty, R.; Brandt, R. E.; Poindexter, J. R.; Lee, Y. S.; Sun, L.; Polizzotti, A.; Park, H. H.; et al. 3.88% Efficient Tin Sulfide Solar Cells Using Congruent Thermal Evaporation. *Adv. Mater.* **2014**, *26* (44), 7488–7492.

(15) Park, H. H.; Heasley, R.; Sun, L.; Steinmann, V.; Jaramillo, R.; Hartman, K.; Chakraborty, R.; Sinsermsuksakul, P.; Chua, D.; Buonassisi, T.; Gordon, R. Co-Optimization of SnS Absorber and Zn(O,S) Buffer Materials for Improved Solar Cells. *Prog. Photovoltaics Res. Appl.* **2015**, *23* (7), 901–908.

(16) Rath, T.; Gury, L.; Sánchez-Molina, I.; Martínez, L.; Haque, S. A. Formation of Porous SnS Nanoplate Networks from Solution and Their Application in Hybrid Solar Cells. *Chem. Commun.* **2015**, *51* (50), 10198–10201.

(17) Devika, M.; Koteeswara Reddy, N.; Venkatramana Reddy, S.; Ramesh, K.; Gunasekhar, K. R. Influence of Rapid Thermal Annealing (RTA) on the Structural and Electrical Properties of SnS Films. *J. Mater. Sci. Mater. Electron.* **2009**, *20* (11), 1129–1134.

(18) MacLachlan, A. J.; Rath, T.; Cappel, U. B.; Dowland, S. A.; Amenitsch, H.; Knall, A.-C.; Buchmaier, C.; Trimmel, G.; Nelson, J.; Haque, S. A. Polymer/Nanocrystal Hybrid Solar Cells: Influence of Molecular Precursor Design on Film Nanomorphology, Charge Generation and Device Performance. *Adv. Funct. Mater.* **2015**, *25* (3), 409–420.

(19) Bansal, N.; O'Mahony, F. T. F.; Lutz, T.; Haque, S. A. Solution Processed Polymer-Inorganic Semiconductor Solar Cells Employing Sb 2 S 3 as a Light Harvesting and Electron Transporting Material. *Adv. Energy Mater.* **2013**, *3* (8), 986–990.

(20) Bansal, N.; Reynolds, L. X.; MacLachlan, A.; Lutz, T.; Ashraf, R. S.; Zhang, W.; Nielsen, C. B.; McCulloch, I.; Rebois, D. G.; Kirchartz, T.; Hill, M; Molloy, K; Nelson, J; Haque, S. Influence of Crystallinity and Energetics on Charge Separation in Polymer–Inorganic Nanocomposite Films for Solar Cells. *Sci. Rep.* **2013**, *3* (1), 1531.

(21) Reynolds, L. X.; Lutz, T.; Dowland, S.; MacLachlan, A.; King, S.; Haque, S. A. Charge Photogeneration in Hybrid Solar Cells: A Comparison between Quantum Dots and in Situ Grown CdS. *Nanoscale* **2012**, *4* (5), 1561.

(22) O'Mahony, F. T. F.; Lutz, T.; Guijarro, N.; Gómez, R.; Haque, S. A. Electron and Hole Transfer at Metal oxide/Sb2S3/spiro-OMeTAD Heterojunctions. *Energy Environ. Sci.* **2012**, *5* (12), 9760.

(23) Cappel, U. B.; Dowland, S. A.; Reynolds, L. X.; Dimitrov, S.; Haque, S. A. Charge Generation Dynamics in CdS:P3HT Blends for Hybrid Solar Cells. *J. Phys. Chem. Lett.* **2013**, *4* (24), 4253–4257.

TOC GRAPHIC